Landslide Volumetric Analysis Using Cartosat-1-Derived DEMs

Tapas R. Martha, Norman Kerle, Victor Jetten, Cees J. van Westen, and K. Vinod Kumar

***Abstract*—The monitoring of landscape changes can lead to the identification of environmental hot spots, improve process understanding, and provide means for law enforcement. Digital elevation models (DEMs) derived from stereoscopic satellite data provide a systematic synoptic framework that is potentially useful to support these issues. Along-track high-resolution stereoscopic data, provided with rational polynomial coefficients (RPCs), are ideal for the fast and accurate extraction of DEMs due to the reduced radiometric differences between images. In this letter, we assess the suitability of data from the relatively new Cartosat-1 satellite to quantify large-scale geomorphological changes, using the volume estimation of the 2007 Salna landslide in the Indian Himalayas as a test case. The depletion and accumulation volumes, estimated as 0.55×10^6 and 1.43×10^6 m^3, respectively, showed a good match with the volumes calculated using DEMs generated only with RPCs and without ground control points (GCPs), indicating that the volume figures are less sensitive to GCP support. The result showed that these data can provide an important input for disaster-management activities.**

***Index Terms*—Cartosat-1, disaster management, landslide, volume estimation.**

I. Introduction

LARGE-SCALE anthropogenic landscape changes, such as those caused by mining and urban waste disposal, and those of natural origin, such as landslides and glacial melting, are primary topographic change drivers [1]–[4]. Small or subtle changes are readily quantified using techniques such as radar interferometry or, where available, laser scanning data. Volumetric analysis has the potential to monitor and quantify also large-scale events and can be useful in implementing proper risk-management strategies or enforcing environmental regulations. For example, reliable information on material volume can help government agencies in estimating the value of contract and the number of days required to clear the debris from transportation routes in case of a landslide [5] or the amount of material required to reclaim the land in case of open-pit mining as a mandatory requirement under a mine control act [6]. In the past, such assessments have typically been done through time-consuming field measurements, although those tend to suffer from difficulties in establishing accurate baseline topography. Photogrammetric techniques have been increasingly used because of their capability to rapidly reconstruct the 3-D topography from aerial photographs [4], [7], [8] and, provided such data exist for different time periods, allow objective change detection. More recently, civilian Earth-observation satellites have offered stereoscopic data with sufficient spatial resolution to allow aerial data to be effectively replaced [9]–[12]. In addition, new-generation satellites such as Cartosat-1 have considerable advantages over airborne stereo imagery, due to their high periodicity, synoptic view, high data quality, relatively low cost, and quick extraction of digital surface models (DSMs) using rational function models (RFMs) [11], [13]. AQ1

Cartosat-1, launched by the Indian Space Research Organisation in 2005, is a global mission planned for cartographic mapping, urban studies, and disaster management [14]. It carries two cameras, PAN-aft and PAN-fore with -5° and $+26^\circ$ viewing angles, respectively, acquiring images of a 900-km^2 area ($12\,000 \times 12\,000$ pixels) with a gap of 52 s. The ground sampling distance of Cartosat-1 is 2.5 m, and the base-to-height ratio is 0.62. Detailed specifications of Cartosat-1 are provided in [14]. Data from Cartosat-1 are 10 b and provided with rational polynomial coefficients (RPCs) for photogrammetric processing and extraction of 3-D information using RFM. In principle, therefore, Cartosat-1 data are well suited for fast and accurate 3-D surface reconstruction, although, in practice, there can be potential problems due to shadows, occlusions, and steep slopes depending on the terrain [11], [13]. With Cartosat-1 acquiring along-track data, image matching is less problematic than that for across-track images due to the reduced radiometric variation between the two images of a stereo pair [10]; however, factors such as valley orientation, sun elevation angle, and poor texture frequently hinder the accurate extraction of elevation data [11]. We addressed some of these problems through the Satellite Image Precision Processing (SAT-PP) photogrammetric software, particularly developed for high-resolution satellite data and which previously demonstrated the ability to process such stereoscopic data due to its superior image-matching algorithm [12] compared with other commercial off-the-shelf (COTS) software types [11]. AQ2

In this letter, we tested the use of Cartosat-1 data for volume analysis based on cut-and-fill assessment, an established method for estimating the volume of large landslides [4], [9], [15]. We used the 2007 Salna landslide in the Indian Himalayas as a test case, which offers a great challenge to automatic digital elevation model (DEM) extraction due to steep slopes and large topographic shadows [11]. Previous studies have demonstrated the utility of DEMs extracted from satellite data for monitoring topographic changes due to glacial melting [3], [8], landslides [9], and rehabilitation planning of coal mining areas [16].

Manuscript received October 5, 2009; revised December 22, 2009.

T. R. Martha is with the National Remote Sensing Centre (NRSC), Indian Space Research Organisation (ISRO), Hyderabad 500 625, India, and also with the International Institute for Geo-Information Science and Earth Observation (ITC), 7500 AA Enschede, The Netherlands (e-mail: tapas_martha@nrsc.gov.in; martha@itc.nl).

N. Kerle, V. Jetten, and C. J. van Westen are with ITC, 7500 AA Enschede, The Netherlands (e-mail: kerle@itc.nl; jetten@itc.nl; westen@itc.nl).

K. Vinod Kumar is with NRSC, ISRO, Hyderabad 500 625, India (e-mail: vinodkumar_k@nrsc.gov.in).

Color versions of one or more of the figures in this paper are available online at http://ieeexplore.ieee.org.

Digital Object Identifier 10.1109/LGRS.2010.2041895

The purpose here is to assess if Cartosat-1-derived DEMs are sufficiently accurate to quantify such changes and to monitor compliance with related legislation.

A. Landslide Volume Estimation

Landslides are major mass-wasting processes and landscape-building factors in mountainous terrains. They are primarily triggered by seismic activity, rainfall, or road construction and cause enormous destruction to properties and lives in those areas. Some of the major earthquakes that have created several deep-seated landslides in the recent past are the Kashmir earthquake in India and Pakistan in October 2005 and the Sichuan earthquake in China in May 2008. Apart from direct damage, landslides also contribute sediments to river systems and create siltation problems in reservoirs, reducing their capacity for hydropower generation. They also have the potential to create artificial lakes by blocking river courses, thus generating potential flash floods in downstream areas [17], [18]. Knowledge of failure volumes is also critical for a more accurate understanding of the landslide process [e.g., [19]] and the preparation of susceptibility maps, which show potential areas of future landslide occurrences. For example, landslide susceptibility maps will be more accurate if volume, instead of the area of the landslide, is used to calculate the weights of the terrain parameters. Okura *et al.* [20] showed how the volume of a landslide directly affects its travel distance, while Dai and Lee [21] demonstrated that frequency–volume relationships can be used to predict rainfall-induced landslides.

Traditionally, failure volumes have been estimated by measuring landslide dimensions (length, width, and depth) on the ground, using assumptions about the shape of the landslide [22]. Such ground-based methods may provide accurate volume figures, although these are time consuming, error prone, and, at times, not possible due to terrain inaccessibility. Pre- and post-failure topographic maps can also be used for calculating the landslide volume using change-detection techniques. However, topographic maps are typically not updated immediately after the event or lack sufficient accuracy [4]. In order to overcome these problems, multitemporal aerial photographs were initially used to estimate landslide extents and volumes [2], [7]. Dewitte and Demoulin [7] generated DEMs with high accuracy from aerial photographs using photogrammetric techniques to estimate the volume of 13 deep-seated landslides in the Flemish Ardennes. However, with advancements in image-processing techniques and increasing availability of high-resolution stereoscopic satellite data, quantitative studies on landform changes using DEMs based on satellite data have become a viable option [23]. Recently, Tsutsui *et al.* [9] used SPOT-5 stereoscopic data and generated 5-m DEMs to calculate the volume of landslides triggered due to an earthquake and a cyclone in Japan and Taiwan, respectively. However, their estimated volume showed a mismatch with the reference volume due to inaccuracies in the DEM resulting from poor texture in 8-b SPOT images and topographic shadow. The problems of poor texture can be reduced by the use of 11-b images from IKONOS or QuickBird [12]. However, their low swath width and high cost render those sensors impractical for routine volumetric analysis. Moreover, prefailure images essential for volume estimation are mostly not available from these satellites. Kerle [4] and Scott *et al.* [19] showed how lack of knowledge of prefailure topography and limited access to the site led to a ground-based volume underestimation of the 1998 flank collapse at the Casita Volcano, Nicaragua, of almost an order of magnitude eight.

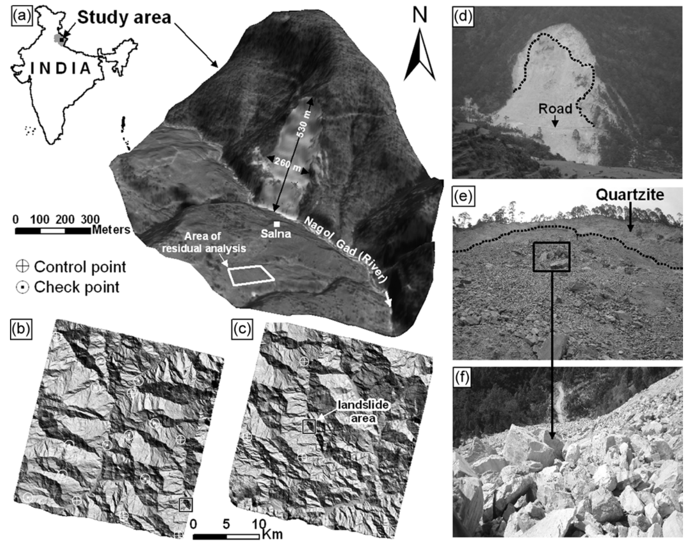

Fig. 1. Location map of the study area. (a) Three-dimensional perspective view of the Salna landslide with the Cartosat-1 image draped over a DEM, (b) and (c) pre- and postlandslide DEMs, respectively, showing the distribution of control and check points, (d) field photograph showing the synoptic view of the landslide, (e) view of the quartzite bedrock exposed in (the area above the black dotted line) the scarp, and a part of the zone of accumulation as seen from the temporarily constructed road, and (f) large angular boulders with large voids in between, signaling a volume increase during deposition.

II. Area and Data Analysis

A. Test Area

The test area is located in one of the landslide-prone areas in the Himalayas (30°23′38″ N and 79°12′42″ E). It is located in the Nagol Gad (River) subcatchment in the High Himalayas in the Uttarakhand state of India (Fig. 1). Nagol Gad is a part of the Alaknanda catchment, which witnessed several major coseismic landslides during the Chamoli earthquake in March 1999 and lies very close to the Main Central Thrust [24]. Rocks such as banded quartzite at the crown, and quartzite interbedded with mica schist at the toe of the landslide, belonging to the Proterozoic era are exposed in this area. However, the landslide investigated for this volumetric analysis was triggered by heavy rainfall in July 2007. It occurred near the Salna village in the Chamoli district of the Uttarakhand state. The landslide-affected area is completely exposed to sun in both pre- and postlandslide images [Fig. 2(a) and (b)]. The general topography is steep, with slopes ranging from 18° to 63°. The elevations of the crown and tip of the landslide are 1636 and 1261 m, respectively. The Salna landslide is a translational rock slide, meaning that the failure has taken place along a planar surface of rupture. Its length (crown to tip) is 530 m, with a maximum width at the center of the landslide of 260 m [Fig. 1(a)]. Although there were no fatalities, the major road connecting the surrounding area with the Chamoli town was blocked for several months, causing hardship to local population and damage to the regional economy.

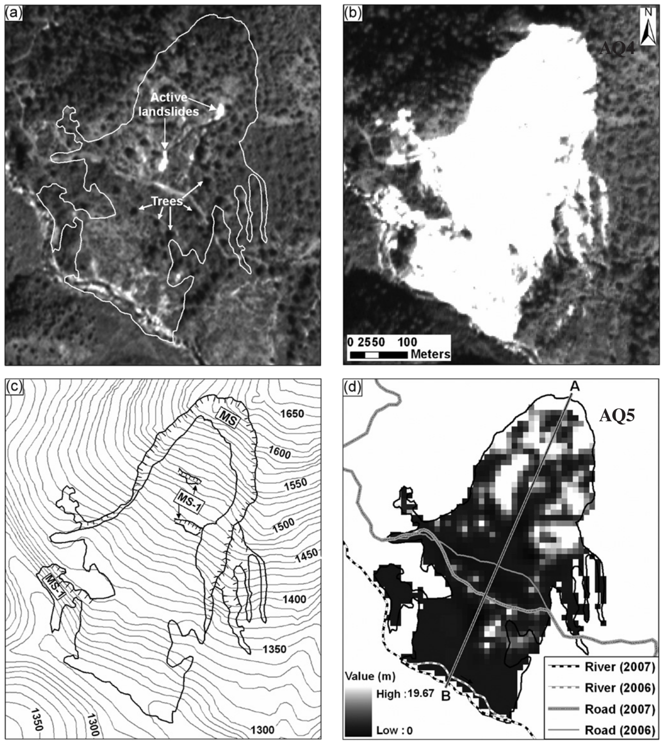

Fig. 2. Salna landslide. (a) Cartosat-1 orthoimage of April 6, 2006, showing the prelandslide area outlined in white. It was a distressed zone with the presence of two minor landslides acting as a precursor to the main event. (b) Cartosat-1 orthoimage of December 16, 2007, showing the landslide that occurred in July 2007. (c) Postlandslide map showing the (MS) main scarp and (MS-1) minor scarps. (d) Nonuniform vegetation-height surface created by the interpolation of heights measured from 74 trees and postlandslide effects. The new road now has a convex outward shape, and the original river was pushed outward due to the deposition of debris at the foothill region. The profile along A–B is shown in Fig. 3.

B. DEM Generation

Two sets of stereoscopic Cartosat-1 data, acquired on April 6, 2006 (prelandslide) and December 16, 2007 (postlandslide), were processed using the SAT-PP software. Compared with established COTS photogrammetric packages, SAT-PP has an improved image-matching algorithm based on the combined matching results of feature points, grid points, and edges, leading to superior results also in steep terrain [11], [12]. DSMs with 10-m grid size were generated using RPCs determined from the RFM and provided by the data vendor. RFM is a generic sensor model and is used as an alternative to physical sensor models for the block orientation of the stereo-image pair. RPCs are terrain independent and require refinement with ground control points (GCPs) at block level to increase the absolute geolocation accuracy of DSMs [13]. Therefore, we used six GCPs with good planimetric and vertical distributions to refine the orientation result of the RFM [Fig. 1(b)] [13]. The GCPs were collected in a differential GPS (DGPS) survey using a dual-frequency (L1 and L2) Leica 520 receiver. The standard deviations of the errors of the elevation, longitude, and latitude of the points surveyed range between 0.10 and 0.46 m, 0.04 and 0.15 m, and 0.04 and 0.21 m, respectively.

The necessity of high DEM accuracy for an elevation-change analysis has been emphasized by previous researchers [4], [25]. Kerle [4] showed how, particularly, the combination of errors in the vertical accuracy of photogrammetrically derived DEMs and the landslide thickness, typically being the smallest dimension, readily combine to produce substantial uncertainty. Errors in the elevation difference can either result from the misregistration of the pre- and postevent DEMs [25] or from the low spatial accuracy resulting from sun illumination and valley orientation with reference to the satellite track [11]. Along-track satellite data such as those from Cartosat-1 offer improved results of image matching due to the reduced radiometric variation between images of a stereo pair [10]. However, the distortion of feature geometry due to the steep terrain and variable viewing angle of Cartosat-1 has compromised some of these advantages. This problem can be overcome using the SAT-PP software, which relies on robust point-, grid-, and feature-based image-matching techniques [12]. Topographic shadow in mountainous areas is another problem that creates inaccuracies in a DEM. SAT-PP is also capable of generating the adequate number of match points required for an accurate DEM generation for relatively small shadow areas; however, large shadows still remain a problem [11], [12].

In an earlier study, we assessed the absolute accuracy of the prelandslide DEM using ten independent check points obtained from the DGPS survey, resulting in vertical and planimetric root-mean-square errors of 2.31 and < 1 m, respectively [11]. In addition, the spatial accuracy of the prelandslide DEM was estimated by a drainage line comparison method, wherein drainage lines were used as a proxy to estimate the error due to spatial autocorrelation in the absence of a very accurate reference DEM [11]. Subsequently, the refinement of the orientation result of postlandslide RFM was done by using three GCPs common in the overlap area [Fig. 1(c)]. Thus, both DEMs were brought into the same spatial framework. However, to verify the vertical and coregistration accuracies of two DEMs, a residual analysis was carried out between the two DEMs in an area adjacent to the landslide [Fig. 1(a)]. This area is unvegetated, and no morphological changes have occurred during the observation period. The residual analysis showed a vertical mean and standard deviation of errors of 0.11 and 0.06 m and corresponding planimetric errors of 0.09 and 0.05 m, respectively. The low errors indicate that both DEMs are coregistered properly and have a good vertical accuracy relative to each other. Therefore, any change in height can be attributed to morphological changes, such as those due to landslides, allowing volumes to be calculated.

C. Volumetric Analysis

As volume calculation must be based on the actual pre- and postlandslide terrain surfaces, vegetation that may have covered the area before failure, or that was possibly retained during the landslide, must be corrected for, as it forms part of the photogrammetric surfaces. The accurate estimation of vegetation height has previously been shown to be challenging [4]. In the area of the Salna landslide, mainly chir trees are found. The height of some of the uprooted and standing trees (in the adjacent area) was measured on the ground. This height, in conjunction with the height of the trees measured through the manual interpretation of stereo images, was used to create a nonuniform vegetation-height surface [Fig. 2(d)]. A total of 74 trees (7 on the ground and 67 in the stereo image) with a mean height of 11.87 m (minimum of 4.29 m and maximum

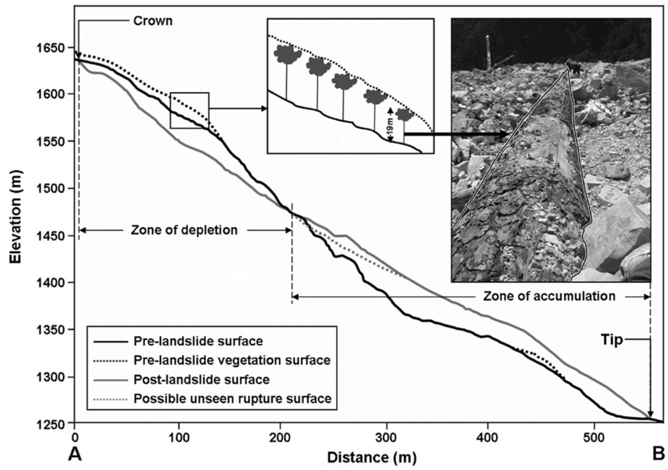

Fig. 3. Pre- and postfailure surface profile from the crown to tip of the landslide. The gray dotted line shows the possible extension of the surface of rupture over which debris is temporarily deposited. The heights of some of the chir pine trees were measured on the ground (e.g., an uprooted tree in the inset photograph).

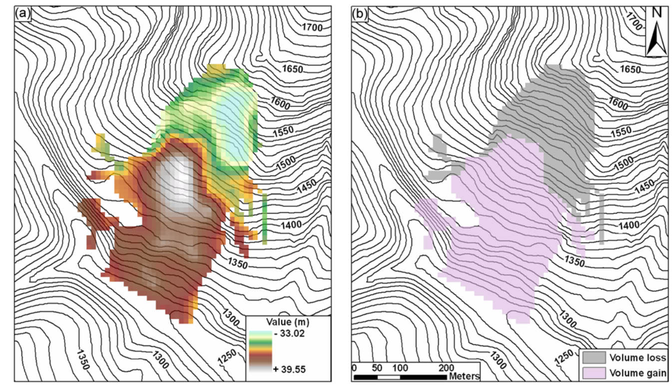

Fig. 4. Volumetric analysis of the Salna landslide. (a) Elevation difference due to landslide with negative values showing the lowering of surface and positive values showing the rising of the surface after the event. (b) Extent of the volume loss and volume gain, which corresponds to the zones of depletion and accumulation, respectively.

TABLE I
QUANTITATIVE COMPARISON OF VOLUME

DEM type	Volume loss (10^6 m^3)		Volume gain (10^6 m^3)		Bulking
	Before vegetation correction	After vegetation correction	Before vegetation correction	After vegetation correction	
DEM (with GCP)	0.77	0.55	1.34	1.43	2.60
DEM (without GCP)	0.76	0.54	1.31	1.41	2.61
DTM (spot height)	0.67		1.26		1.88

of 19.67 m) were used for the creation of the nonuniform vegetation-height surface. Subsequently, this surface was subtracted from the automatically generated prefailure DSM, and a vegetation-corrected digital terrain model (DTM) was created. Vegetation correction was not required for the postfailure DSM since trees were completely uprooted. After vegetation correction, the area and volume of the Salna landslide were calculated by subtracting the postlandslide DTM from the prelandslide DTM, using the cut-and-fill operation in ArcGIS. This operation summarizes the areas and volumes of change using the surfaces of a given location at two different time periods and identifies regions of surface-material removal and addition and no change.

III. RESULTS AND DISCUSSION

The Salna landslide was triggered due to excessive rainfall, and the prelandslide Cartosat-1 image already showed the existence of small active landslides in the area [Fig. 2(a)]. The slope length of the main scarp below the crown of the landslide is approximately 50 m [Fig. 2(c)]. The landslide completely buried the road with material displaced from the crown part. The new road [Fig. 1(d)], which was temporarily constructed to allow traffic to resume, is now positioned 62 m outward from its previous location, and the shape of the road is convex outward [Fig. 2(d)], indicating the deposition of a large amount of material and the development of a hummocky structure. Similarly, the Nagol Gad (River) was pushed 25 m to its right bank by the landslide [Fig. 2(d)]. Fortunately, no damming of the river occurred due to the landslide. Debris mainly composed of boulders of banded quartzite is seen in the zone of accumulation [Fig. 1(e) and (f)].

From the profile (Fig. 3) and from the extent of the volume gain [Fig. 4(b)], it is clear that the area of the zone of depletion is smaller than the area of the zone of accumulation, indicating expansion, or bulking, of material after the displacement due to the fragmentation of the bed rock. The elevation-change map shows that maximum deposition of material has taken place at a height of approximately 1420 m [Fig. 4(a)]. The cut-and-fill volumes, i.e., the volumes of depleted and accumulated material, were estimated as 0.55×10^6 and 1.43×10^6 m^3, respectively (Table I).

So far, we have estimated the landslide volume from DEMs derived with the use of additional GCPs. However, the need for field-measured control points, a strict requirement in traditional photogrammetry, severely undermines the utility of satellite data for rapid and independent postlandslide assessment. To assess the dependence of accurate volume estimation on additional field-mapped GCPs, we also created DEMs only with the RPCs provided with Cartosat-1 data. Such a step is reasonable, as additional GCPs primarily affect the absolute accuracy of the DEM and lessen the relative elevation value distribution. Nevertheless, the effect of integrating two such relative surfaces for accurate change assessment was unknown. Table I shows that the estimated volume values based on RPC-only DEMs fall to within 1%–3% of the GCP-supported DEM values, indicating that the volume figures are less sensitive to GCP support than expected.

The bulking factor (ratio of volume gain to volume loss) of 2.60 (Table I) is comparable with previously reported values for similar events, such as the bulking following the flank collapse of the Casita Volcano, Nicaragua, studied by Scott *et al.* [19]. The bulking of the Salna landslide is due to two factors: 1) incomplete separation of loss area from gain area, due to which the material is still lying at the bottom of the hidden rupture surface [2], which is impossible to be reconstructed from postfailure stereo data (Fig. 3), and 2) poor sorting of large and angular broken quartzite rock fragments [Fig. 1(f)] created by the translational rock slide, leading to a possible overestimation of the gain volume. However, the estimated volume can be considered realistic, since the postlandslide surface was generated shortly (approximately five months) after the occurrence of the landslide, suggesting limited deposition material loss due to surface erosion and further remobilization.

A. *Accuracy Assessment of Volume*

The global accuracy of the DEM has been verified by independent check points, although previous studies have shown that digital photogrammetry with low global errors can still lead to substantial local errors, particularly in areas of low contrast (e.g., uniform vegetation and landslide failure flanks). Volume accuracy assessment in such small local areas is thus a challenge, particularly with only limited reference data, i.e., without a dense network of ground check points for both pre- and postlandslide affected areas. Due to the absence of detailed verification data for the relatively small landslide area (i.e., part of the large DEMs for which accuracy has been checked), we manually extracted spot heights [4], identifying 85 and 129 points from the pre- and postfailure data sets, respectively, using StereoAnalyst in ERDAS Imagine, and compared the volume obtained from spot-height data with the automatic results (Table I). The number of points is sufficient for a reliable comparison since they were collected with particular emphasis on break-in-slope and scarp areas, leading to a surface that models the actual failure area well. Spot heights from the prefailure image were collected by selectively measuring ground elevations in between trees, thus eliminating the need for further vegetation correction, and directly on the failure and deposition surfaces in the postfailure image. These points were interpolated using the TOPOGRID algorithm in ArcGIS to derive reference DTMs [26].

IV. Conclusion

Updated elevation data are essential for identifying areas of large-scale topographic changes for disaster management or enforcement of environmental legislation. The purpose of this letter was to assess the potential of a new generation of spaceborne sensors to provide DEMs for the quantification of landscape changes. In this letter, DEMs with 10-m grid size corresponding to two different time periods, generated from Cartosat-1 data using digital photogrammetric methods, were used to quantify large-scale topographic changes resulting from a landslide. Following photogrammetric conventions, we generated DEMs with a grid size equivalent to three to four times of the ground sampling distance. With some data types, such as from SPOT-5, higher resolutions can be achieved, for example, the 2.5-m resolution DEMs produced by Tsutsui *et al.* [9], using superresolution processing [27]. Interestingly, the previously reported requirement for additional GCPs [13] was found to be of lesser importance, allowing us to create surfaces with comparable relative accuracy also without such field-based measurements. This requires the actual coregistration of pre- and postfailure DSMs rather than the use of absolute coordinates. This means that RPCs alone are sufficient for the estimation of volume, thus freeing rapid postfailure volume assessment entirely from field data requirements, although the refinement of the RFM orientation result is required to improve the absolute geolocation accuracy necessary for cartographic applications. Knowledge on prefailure topography is crucial for the accurate estimation of volume [4]. Cartosat-1 was launched in 2005, and its data were systematically acquired, providing substantial archives of images for major parts of the world. The availability of postfailure data sets from Cartosat-1 shortly after the event then enabled us to do rapid volume estimation. The cut-and-fill volumes derived from automatic DEMs showed a reasonably good match with the reference volume derived from DEMs generated using manually extracted spot-height data. This indicates that a 10-m DEM from Cartosat-1 data can be effectively used for large-scale elevation change and volumetric analysis such as that for a deep-seated landslide. The information on landslide volume can effectively be used to establish magnitude–frequency relationship for quantitative estimation of a landslide hazard. However, the volume values calculated based on manually extracted spot heights show deviations of about +18% and −12% for the volume loss and gain areas, respectively, resulting also in a bulking factor that is 27% lower than that based on automatic DEMs with GCPs. These deviations of volume values can be attributed to the steep slope (51°) near the crown of the landslide, where automatically generated DEMs are prone to error [9].

This letter has shown that Cartosat-1 data have the potential to derive volume information critical for disaster assessment, in principle, without any additional GPS field measurement, provided that any present vegetation artifacts are removed from the DEMs used in the change assessment. It must also be noted that, with landslide thickness, i.e., z, typically being the smallest dimension, elevation errors resulting from photogrammetric artifacts or inaccurate DSM-to-DTM correction will have a correspondingly large consequence on volume calculations. The quantitative estimation of similar large-scale changes in the landscape, e.g., due to open-pit mining and urban waste disposal, although not shown in this letter, can, in principle, also be done with Cartosat-1-derived DEMs since they require multitemporal DEMs similar to the ones used in this letter.

References

[1] T. R. Martha, A. Guha, K. Vinod Kumar, M. V. V. Kamaraju, and E. V. R. Raju, "Recent coal fire and land use status of Jharia Coalfield, India from satellite data," *Int. J. Remote Sens.*, to be published, to be published. AQ9

[2] C. J. van Westen and F. Lulie Getahun, "Analyzing the evolution of the Tessina landslide using aerial photographs and digital elevation models," *Geomorphology*, vol. 54, no. 1/2, pp. 77–89, Aug. 15, 2003.

[3] A. B. Surazakov and V. B. Aizen, "Estimating volume change of mountain glaciers using SRTM and map-based topographic data," *IEEE Trans. Geosci. Remote Sens.*, vol. 44, no. 10, pp. 2991–2995, Oct. 2006.

[4] N. Kerle, "Volume estimation of the 1998 flank collapse at Casita volcano, Nicaragua: A comparison of photogrammetric and conventional techniques," *Earth Surf. Process. Landforms*, vol. 27, no. 7, pp. 759–772, Jul. 2002.

[5] P. Jaiswal and C. J. van Westen, "Estimating temporal probability for landslide initiation along transportation routes based on rainfall thresholds," *Geomorphology*, vol. 112, no. 1/2, pp. 96–105, Nov. 2009.

[6] P. A. Townsend, D. P. Helmers, C. C. Kingdon, B. E. McNeil, K. M. de Beurs, and K. N. Eshleman, "Changes in the extent of surface mining and reclamation in the Central Appalachians detected using a 1976–2006 Landsat time series," *Remote Sens. Environ.*, vol. 113, no. 1, pp. 62–72, Jan. 2009.

[7] O. Dewitte and A. Demoulin, "Morphometry and kinematics of landslides inferred from precise DTMs in West Belgium," *Natural Hazards Earth Syst. Sci.*, vol. 5, no. 2, pp. 259–265, 2005.

[8] A. Kääb, "Monitoring high-mountain terrain deformation from repeated air- and spaceborne optical data: Examples using digital aerial imagery and ASTER data," *ISPRS J. Photogramm. Remote Sens.*, vol. 57, no. 1/2, pp. 39–52, Nov. 2002.

[9] K. Tsutsui, S. Rokugawa, H. Nakagawa, S. Miyazaki, C. T. Cheng, T. Shiraishi, and S. D. Yang, "Detection and volume estimation of large-scale landslides based on elevation-change analysis using DEMs extracted from high-resolution satellite stereo imagery," *IEEE Trans. Geosci. Remote Sens.*, vol. 45, no. 6, pp. 1681–1696, Jun. 2007.

[10] V. N. Radhika, B. Kartikeyan, B. Gopala Krishna, S. Chowdhury, and P. K. Srivastava, "Robust stereo image matching for spaceborne imagery," *IEEE Trans. Geosci. Remote Sens.*, vol. 45, no. 9, pp. 2993–3000, Sep. 2007.

[11] T. R. Martha, N. Kerle, C. J. van Westen, V. Jetten, and K. Vinod Kumar, "Effect of sun elevation angle on DSMs derived from Cartosat-1 data," *Photogramm. Eng. Remote Sens.*, to be published, to be published. AQ10

[12] L. Zhang and A. Gruen, "Multi-image matching for DSM generation from IKONOS imagery," *ISPRS J. Photogramm. Remote Sens.*, vol. 60, no. 3, pp. 195–211, May 2006.

[13] E. Baltsavias, S. Kocaman, and K. Wolff, "Analysis of Cartosat-1 images regarding image quality, 3D point measurement and DSM generation," *Photogramm. Rec.*, vol. 23, no. 123, pp. 305–322, Sep. 2008.

[14] *Cartosat-1 Data User's Handbook*, NRSC, Hyderabad, India, [Online]. Available: http://www.nrsa.gov.in/IRS_Documents/Handbook/cartosat1.pdf AQ11

[15] R.-F. Chen, Y.-C. Chan, J. Angelier, J.-C. Hu, C. Huang, K.-J. Chang, and T.-Y. Shih, "Large earthquake-triggered landslides and mountain belt erosion: The Tsaoling case, Taiwan," *Comptes Rendus Geosci.*, vol. 337, no. 13, pp. 1164–1172, Sep./Oct. 2005.

[16] D. Loczy, S. Czigany, J. Dezso, P. Gyenizse, J. Kovacs, L. Nagyvaradi, and E. Pirkhoffer, "Geomorphological tasks in planning the rehabilitation of coal mining areas at Pecs, Hungary," *Geografia Fisica E Dinamica Quaternaria*, vol. 30, no. 2, pp. 203–207, 2007.

[17] S. A. Dunning, W. A. Mitchell, N. J. Rosser, and D. N. Petley, "The Hattian Bala rock avalanche and associated landslides triggered by the Kashmir Earthquake of 8 October 2005," *Eng. Geol.*, vol. 93, no. 3/4, pp. 130–144, Aug. 2007.

[18] F. Wang, Q. Cheng, L. Highland, M. Miyajima, H. Wang, and C. Yan, "Preliminary investigation of some large landslides triggered by the 2008 Wenchuan earthquake, Sichuan Province, China," *Landslides*, vol. 6, no. 1, pp. 47–54, Mar. 2009.

[19] K. M. Scott, J. W. Vallance, N. Kerle, J. L. Macías, W. Strauch, and G. Devoli, "Catastrophic precipitation-triggered lahar at Casita volcano, Nicaragua: Occurrence, bulking and transformation," *Earth Surf. Process. Landforms*, vol. 30, no. 1, pp. 59–79, Jan. 2005.

[20] Y. Okura, H. Kitahara, A. Kawanami, and U. Kurokawa, "Topography and volume effects on travel distance of surface failure," *Eng. Geol.*, vol. 67, no. 3/4, pp. 243–254, Jan. 2003.

[21] F. C. Dai and C. F. Lee, "Frequency-volume relation and prediction of rainfall-induced landslides," *Eng. Geol.*, vol. 59, no. 3/4, pp. 253–266, Apr. 2001.

[22] D. Cruden and D. J. Varnes, "Landslide types and processes," in *Landslides Investigation and Mitigation, Special Report 247*, A. K. Turner and R. L. Schuster, Eds. Washington, DC: Transp. Res. Board, Nat. Acad. Sci., 1996, pp. 36–75.

[23] J. Chandler, "Effective application of automated digital photogrammetry for geomorphological research," *Earth Surf. Process. Landforms*, vol. 24, no. 1, pp. 51–63, Jan. 1999.

[24] P. L. Barnard, L. A. Owen, M. C. Sharma, and R. C. Finkel, "Natural and human-induced landsliding in the Garhwal Himalaya of northern India," *Geomorphology*, vol. 40, no. 1/2, pp. 21–35, Sep. 2001.

[25] T. G. Van Niel, T. R. McVicar, L. Li, J. C. Gallant, and Q. Yang, "The impact of misregistration on SRTM and DEM image differences," *Remote Sens. Environ.*, vol. 112, no. 5, pp. 2430–2442, May 2008.

[26] S. M. Wise, "Effect of differing DEM creation methods on the results from a hydrological model," *Comput. Geosci.*, vol. 33, no. 10, pp. 1351–1365, Oct. 2007.

[27] C. Latry and B. Rouge, "Super resolution: Quincunx sampling and fusion processing," in *Proc. Int. Geosci. Remote Sens. Symp.*, 2003, pp. 315–317.

AUTHOR QUERIES

AUTHOR PLEASE ANSWER ALL QUERIES

The paper exceeds the maximum allowable number of pages. Please shorten the paper to fit into five pages.

AQ1 = “DEM” was changed to “DSMs.” Please check if appropriate.
AQ2 = “SAT-PP” was defined as “Satellite Image Precision Processing.” Please check.
AQ3 = This sentence was reworded for clarity purposes. Please check if the original meaning was retained.
AQ4 = Kindly check if the intended meaning of this sentence was achieved.
AQ5 = Please check if the original meaning of this sentence was retained.
AQ6 = Please provide the definition of “GSI.”
AQ7 = Please provide the expanded form of “RS&GIS-AA,” if applicable.
AQ8 = “ETH” was defined as “Eidgenössische Technische Hochschule.” Please check.
AQ9 = Please provide publication update for Ref. [1].
AQ10 = Please provide publication update for Ref. [11].
AQ11 = Please provide year of publication in Ref. [14].
NOTE: Please check the URL provided in Ref. [14]. The page could not be found.

END OF ALL QUERIES

Landslide Volumetric Analysis Using Cartosat-1-Derived DEMs

Tapas R. Martha, Norman Kerle, Victor Jetten, Cees J. van Westen, and K. Vinod Kumar

***Abstract*—The monitoring of landscape changes can lead to the identification of environmental hot spots, improve process understanding, and provide means for law enforcement. Digital elevation models (DEMs) derived from stereoscopic satellite data provide a systematic synoptic framework that is potentially useful to support these issues. Along-track high-resolution stereoscopic data, provided with rational polynomial coefficients (RPCs), are ideal for the fast and accurate extraction of DEMs due to the reduced radiometric differences between images. In this letter, we assess the suitability of data from the relatively new Cartosat-1 satellite to quantify large-scale geomorphological changes, using the volume estimation of the 2007 Salna landslide in the Indian Himalayas as a test case. The depletion and accumulation volumes, estimated as 0.55×10^6 and 1.43×10^6 m^3, respectively, showed a good match with the volumes calculated using DEMs generated only with RPCs and without ground control points (GCPs), indicating that the volume figures are less sensitive to GCP support. The result showed that these data can provide an important input for disaster-management activities.**

***Index Terms*—Cartosat-1, disaster management, landslide, volume estimation.**

I. Introduction

LARGE-SCALE anthropogenic landscape changes, such as those caused by mining and urban waste disposal, and those of natural origin, such as landslides and glacial melting, are primary topographic change drivers [1]–[4]. Small or subtle changes are readily quantified using techniques such as radar interferometry or, where available, laser scanning data. Volumetric analysis has the potential to monitor and quantify also large-scale events and can be useful in implementing proper risk-management strategies or enforcing environmental regulations. For example, reliable information on material volume can help government agencies in estimating the value of contract and the number of days required to clear the debris from transportation routes in case of a landslide [5] or the amount of material required to reclaim the land in case of open-pit mining as a mandatory requirement under a mine control act [6]. In the past, such assessments have typically been done through time-consuming field measurements, although those tend to suffer from difficulties in establishing accurate baseline topography. Photogrammetric techniques have been increasingly used because of their capability to rapidly reconstruct the 3-D topography from aerial photographs [4], [7], [8] and, provided such data exist for different time periods, allow objective change detection. More recently, civilian Earth-observation satellites have offered stereoscopic data with sufficient spatial resolution to allow aerial data to be effectively replaced [9]–[12]. In addition, new-generation satellites such as Cartosat-1 have considerable advantages over airborne stereo imagery, due to their high periodicity, synoptic view, high data quality, relatively low cost, and quick extraction of digital surface models (DSMs) using rational function models (RFMs) [11], [13]. AQ1

Cartosat-1, launched by the Indian Space Research Organisation in 2005, is a global mission planned for cartographic mapping, urban studies, and disaster management [14]. It carries two cameras, PAN-aft and PAN-fore with $-5°$ and $+26°$ viewing angles, respectively, acquiring images of a 900-km^2 area (12 000 × 12 000 pixels) with a gap of 52 s. The ground sampling distance of Cartosat-1 is 2.5 m, and the base-to-height ratio is 0.62. Detailed specifications of Cartosat-1 are provided in [14]. Data from Cartosat-1 are 10 b and provided with rational polynomial coefficients (RPCs) for photogrammetric processing and extraction of 3-D information using RFM. In principle, therefore, Cartosat-1 data are well suited for fast and accurate 3-D surface reconstruction, although, in practice, there can be potential problems due to shadows, occlusions, and steep slopes depending on the terrain [11], [13]. With Cartosat-1 acquiring along-track data, image matching is less problematic than that for across-track images due to the reduced radiometric variation between the two images of a stereo pair [10]; however, factors such as valley orientation, sun elevation angle, and poor texture frequently hinder the accurate extraction of elevation data [11]. We addressed some of these problems through the Satellite Image Precision Processing (SAT-PP) photogrammetric software, AQ2 particularly developed for high-resolution satellite data and which previously demonstrated the ability to process such stereoscopic data due to its superior image-matching algorithm [12] compared with other commercial off-the-shelf (COTS) software types [11].

In this letter, we tested the use of Cartosat-1 data for volume analysis based on cut-and-fill assessment, an established method for estimating the volume of large landslides [4], [9], [15]. We used the 2007 Salna landslide in the Indian Himalayas as a test case, which offers a great challenge to automatic digital elevation model (DEM) extraction due to steep slopes and large topographic shadows [11]. Previous studies have demonstrated the utility of DEMs extracted from satellite data for monitoring topographic changes due to glacial melting [3], [8], landslides [9], and rehabilitation planning of coal mining areas [16].

Manuscript received October 5, 2009; revised December 22, 2009.

T. R. Martha is with the National Remote Sensing Centre (NRSC), Indian Space Research Organisation (ISRO), Hyderabad 500 625, India, and also with the International Institute for Geo-Information Science and Earth Observation (ITC), 7500 AA Enschede, The Netherlands (e-mail: tapas_martha@nrsc.gov.in; martha@itc.nl).

N. Kerle, V. Jetten, and C. J. van Westen are with ITC, 7500 AA Enschede, The Netherlands (e-mail: kerle@itc.nl; jetten@itc.nl; westen@itc.nl).

K. Vinod Kumar is with NRSC, ISRO, Hyderabad 500 625, India (e-mail: vinodkumar_k@nrsc.gov.in).

Color versions of one or more of the figures in this paper are available online at http://ieeexplore.ieee.org.

Digital Object Identifier 10.1109/LGRS.2010.2041895

The purpose here is to assess if Cartosat-1-derived DEMs are sufficiently accurate to quantify such changes and to monitor compliance with related legislation.

A. Landslide Volume Estimation

Landslides are major mass-wasting processes and landscape-building factors in mountainous terrains. They are primarily triggered by seismic activity, rainfall, or road construction and cause enormous destruction to properties and lives in those areas. Some of the major earthquakes that have created several deep-seated landslides in the recent past are the Kashmir earthquake in India and Pakistan in October 2005 and the Sichuan earthquake in China in May 2008. Apart from direct damage, landslides also contribute sediments to river systems and create siltation problems in reservoirs, reducing their capacity for hydropower generation. They also have the potential to create artificial lakes by blocking river courses, thus generating potential flash floods in downstream areas [17], [18]. Knowledge of failure volumes is also critical for a more accurate understanding of the landslide process [e.g., [19]] and the preparation of susceptibility maps, which show potential areas of future landslide occurrences. For example, landslide susceptibility maps will be more accurate if volume, instead of the area of the landslide, is used to calculate the weights of the terrain parameters. Okura *et al.* [20] showed how the volume of a landslide directly affects its travel distance, while Dai and Lee [21] demonstrated that frequency–volume relationships can be used to predict rainfall-induced landslides.

Traditionally, failure volumes have been estimated by measuring landslide dimensions (length, width, and depth) on the ground, using assumptions about the shape of the landslide [22]. Such ground-based methods may provide accurate volume figures, although these are time consuming, error prone, and, at times, not possible due to terrain inaccessibility. Pre- and post-failure topographic maps can also be used for calculating the landslide volume using change-detection techniques. However, topographic maps are typically not updated immediately after the event or lack sufficient accuracy [4]. In order to overcome these problems, multitemporal aerial photographs were initially used to estimate landslide extents and volumes [2], [7]. Dewitte and Demoulin [7] generated DEMs with high accuracy from aerial photographs using photogrammetric techniques to estimate the volume of 13 deep-seated landslides in the Flemish Ardennes. However, with advancements in image-processing techniques and increasing availability of high-resolution stereoscopic satellite data, quantitative studies on landform changes using DEMs based on satellite data have become a viable option [23]. Recently, Tsutsui *et al.* [9] used SPOT-5 stereoscopic data and generated 5-m DEMs to calculate the volume of landslides triggered due to an earthquake and a cyclone in Japan and Taiwan, respectively. However, their estimated volume showed a mismatch with the reference volume due to inaccuracies in the DEM resulting from poor texture in 8-b SPOT images and topographic shadow. The problems of poor texture can be reduced by the use of 11-b images from IKONOS or QuickBird [12]. However, their low swath width and high cost render those sensors impractical for routine volumetric analysis. Moreover, prefailure images essential for volume estimation are mostly not available from these satellites. Kerle [4] and Scott *et al.* [19] showed how lack of knowledge of prefailure topography and limited access to the site led to a ground-based volume underestimation of the 1998 flank collapse at the Casita Volcano, Nicaragua, of almost an order of magnitude eight.

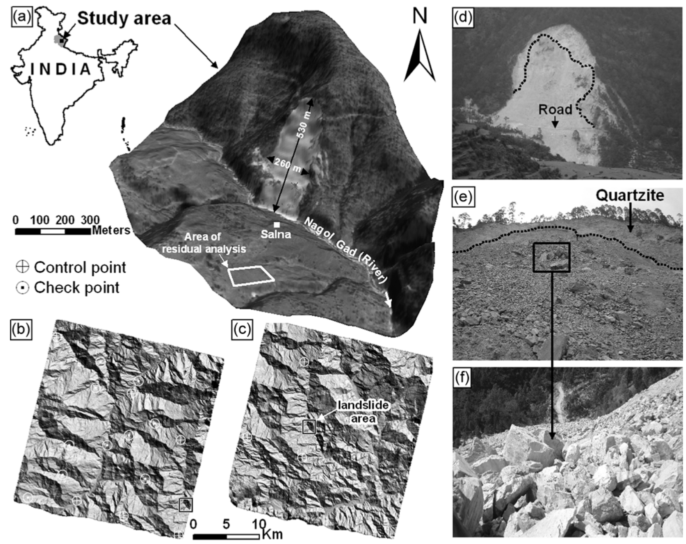

Fig. 1. Location map of the study area. (a) Three-dimensional perspective view of the Salna landslide with the Cartosat-1 image draped over a DEM, (b) and (c) pre- and postlandslide DEMs, respectively, showing the distribution of control and check points, (d) field photograph showing the synoptic view of the landslide, (e) view of the quartzite bedrock exposed in (the area above the black dotted line) the scarp, and a part of the zone of accumulation as seen from the temporarily constructed road, and (f) large angular boulders with large voids in between, signaling a volume increase during deposition.

II. Area and Data Analysis

A. Test Area

The test area is located in one of the landslide-prone areas in the Himalayas (30°23′38″ N and 79°12′42″ E). It is located in the Nagol Gad (River) subcatchment in the High Himalayas in the Uttarakhand state of India (Fig. 1). Nagol Gad is a part of the Alaknanda catchment, which witnessed several major coseismic landslides during the Chamoli earthquake in March 1999 and lies very close to the Main Central Thrust [24]. Rocks such as banded quartzite at the crown, and quartzite interbedded with mica schist at the toe of the landslide, belonging to the Proterozoic era are exposed in this area. However, the landslide investigated for this volumetric analysis was triggered by heavy rainfall in July 2007. It occurred near the Salna village in the Chamoli district of the Uttarakhand state. The landslide-affected area is completely exposed to sun in both pre- and postlandslide images [Fig. 2(a) and (b)]. The general topography is steep, with slopes ranging from 18° to 63°. The elevations of the crown and tip of the landslide are 1636 and 1261 m, respectively. The Salna landslide is a translational rock slide, meaning that the failure has taken place along a planar surface of rupture. Its length (crown to tip) is 530 m, with a maximum width at the center of the landslide of 260 m [Fig. 1(a)]. Although there were no fatalities, the major road connecting the surrounding area with the Chamoli town was blocked for several months, causing hardship to local population and damage to the regional economy.

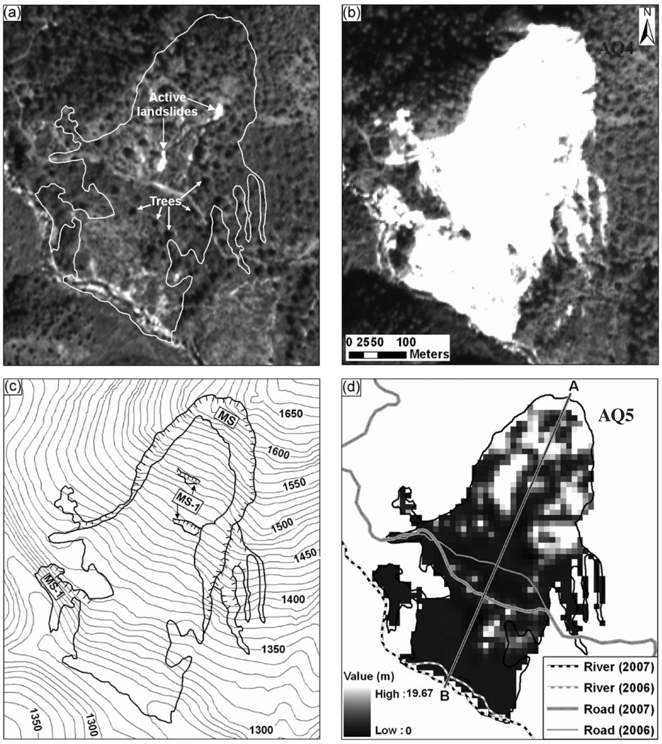

Fig. 2. Salna landslide. (a) Cartosat-1 orthoimage of April 6, 2006, showing the prelandslide area outlined in white. It was a distressed zone with the presence of two minor landslides acting as a precursor to the main event. (b) Cartosat-1 orthoimage of December 16, 2007, showing the landslide that occurred in July 2007. (c) Postlandslide map showing the (MS) main scarp and (MS-1) minor scarps. (d) Nonuniform vegetation-height surface created by the interpolation of heights measured from 74 trees and postlandslide effects. The new road now has a convex outward shape, and the original river was pushed outward due to the deposition of debris at the foothill region. The profile along A–B is shown in Fig. 3.

B. DEM Generation

Two sets of stereoscopic Cartosat-1 data, acquired on April 6, 2006 (prelandslide) and December 16, 2007 (postlandslide), were processed using the SAT-PP software. Compared with established COTS photogrammetric packages, SAT-PP has an improved image-matching algorithm based on the combined matching results of feature points, grid points, and edges, leading to superior results also in steep terrain [11], [12]. DSMs with 10-m grid size were generated using RPCs determined from the RFM and provided by the data vendor. RFM is a generic sensor model and is used as an alternative to physical sensor models for the block orientation of the stereo-image pair. RPCs are terrain independent and require refinement with ground control points (GCPs) at block level to increase the absolute geolocation accuracy of DSMs [13]. Therefore, we used six GCPs with good planimetric and vertical distributions to refine the orientation result of the RFM [Fig. 1(b)] [13]. The GCPs were collected in a differential GPS (DGPS) survey using a dual-frequency (L1 and L2) Leica 520 receiver. The standard deviations of the errors of the elevation, longitude, and latitude of the points surveyed range between 0.10 and 0.46 m, 0.04 and 0.15 m, and 0.04 and 0.21 m, respectively.

The necessity of high DEM accuracy for an elevation-change analysis has been emphasized by previous researchers [4], [25]. Kerle [4] showed how, particularly, the combination of errors in the vertical accuracy of photogrammetrically derived DEMs and the landslide thickness, typically being the smallest dimension, readily combine to produce substantial uncertainty. Errors in the elevation difference can either result from the misregistration of the pre- and postevent DEMs [25] or from the low spatial accuracy resulting from sun illumination and valley orientation with reference to the satellite track [11]. Along-track satellite data such as those from Cartosat-1 offer improved results of image matching due to the reduced radiometric variation between images of a stereo pair [10]. However, the distortion of feature geometry due to the steep terrain and variable viewing angle of Cartosat-1 has compromised some of these advantages. This problem can be overcome using the SAT-PP software, which relies on robust point-, grid-, and feature-based image-matching techniques [12]. Topographic shadow in mountainous areas is another problem that creates inaccuracies in a DEM. SAT-PP is also capable of generating the adequate number of match points required for an accurate DEM generation for relatively small shadow areas; however, large shadows still remain a problem [11], [12].

In an earlier study, we assessed the absolute accuracy of the prelandslide DEM using ten independent check points obtained from the DGPS survey, resulting in vertical and planimetric root-mean-square errors of 2.31 and < 1 m, respectively [11]. In addition, the spatial accuracy of the prelandslide DEM was estimated by a drainage line comparison method, wherein drainage lines were used as a proxy to estimate the error due to spatial autocorrelation in the absence of a very accurate reference DEM [11]. Subsequently, the refinement of the orientation result of postlandslide RFM was done by using three GCPs common in the overlap area [Fig. 1(c)]. Thus, both DEMs were brought into the same spatial framework. However, to verify the vertical and coregistration accuracies of two DEMs, a residual analysis was carried out between the two DEMs in an area adjacent to the landslide [Fig. 1(a)]. This area is unvegetated, and no morphological changes have occurred during the observation period. The residual analysis showed a vertical mean and standard deviation of errors of 0.11 and 0.06 m and corresponding planimetric errors of 0.09 and 0.05 m, respectively. The low errors indicate that both DEMs are coregistered properly and have a good vertical accuracy relative to each other. Therefore, any change in height can be attributed to morphological changes, such as those due to landslides, allowing volumes to be calculated.

C. Volumetric Analysis

As volume calculation must be based on the actual pre- and postlandslide terrain surfaces, vegetation that may have covered the area before failure, or that was possibly retained during the landslide, must be corrected for, as it forms part of the photogrammetric surfaces. The accurate estimation of vegetation height has previously been shown to be challenging [4]. In the area of the Salna landslide, mainly chir trees are found. The height of some of the uprooted and standing trees (in the adjacent area) was measured on the ground. This height, in conjunction with the height of the trees measured through the manual interpretation of stereo images, was used to create a nonuniform vegetation-height surface [Fig. 2(d)]. A total of 74 trees (7 on the ground and 67 in the stereo image) with a mean height of 11.87 m (minimum of 4.29 m and maximum

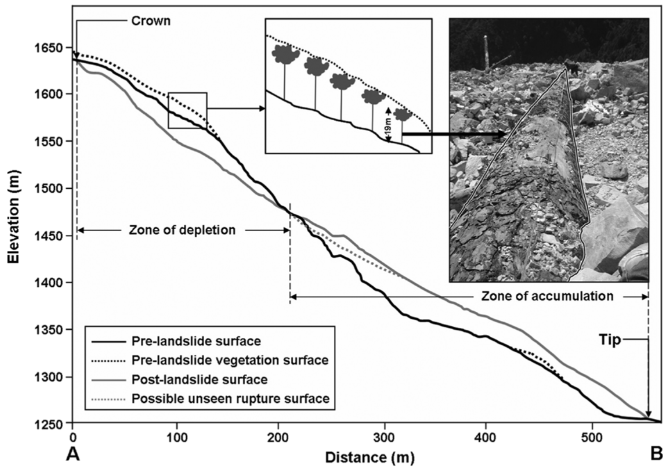

Fig. 3. Pre- and postfailure surface profile from the crown to tip of the landslide. The gray dotted line shows the possible extension of the surface of rupture over which debris is temporarily deposited. The heights of some of the chir pine trees were measured on the ground (e.g., an uprooted tree in the inset photograph).

of 19.67 m) were used for the creation of the nonuniform vegetation-height surface. Subsequently, this surface was subtracted from the automatically generated prefailure DSM, and a vegetation-corrected digital terrain model (DTM) was created. Vegetation correction was not required for the postfailure DSM since trees were completely uprooted. After vegetation correction, the area and volume of the Salna landslide were calculated by subtracting the postlandslide DTM from the prelandslide DTM, using the cut-and-fill operation in ArcGIS. This operation summarizes the areas and volumes of change using the surfaces of a given location at two different time periods and identifies regions of surface-material removal and addition and no change.

III. Results and Discussion

The Salna landslide was triggered due to excessive rainfall, and the prelandslide Cartosat-1 image already showed the existence of small active landslides in the area [Fig. 2(a)]. The slope length of the main scarp below the crown of the landslide is approximately 50 m [Fig. 2(c)]. The landslide completely buried the road with material displaced from the crown part. The new road [Fig. 1(d)], which was temporarily constructed to allow traffic to resume, is now positioned 62 m outward from its previous location, and the shape of the road is convex outward [Fig. 2(d)], indicating the deposition of a large amount of material and the development of a hummocky structure. Similarly, the Nagol Gad (River) was pushed 25 m to its right bank by the landslide [Fig. 2(d)]. Fortunately, no damming of the river occurred due to the landslide. Debris mainly composed of boulders of banded quartzite is seen in the zone of accumulation [Fig. 1(e) and (f)].

From the profile (Fig. 3) and from the extent of the volume gain [Fig. 4(b)], it is clear that the area of the zone of depletion is smaller than the area of the zone of accumulation, indicating expansion, or bulking, of material after the displacement due to the fragmentation of the bed rock. The elevation-change map shows that maximum deposition of material has taken place at a height of approximately 1420 m [Fig. 4(a)]. The cut-and-fill volumes, i.e., the volumes of depleted and accumulated material, were estimated as 0.55×10^6 and 1.43×10^6 m^3, respectively (Table I).

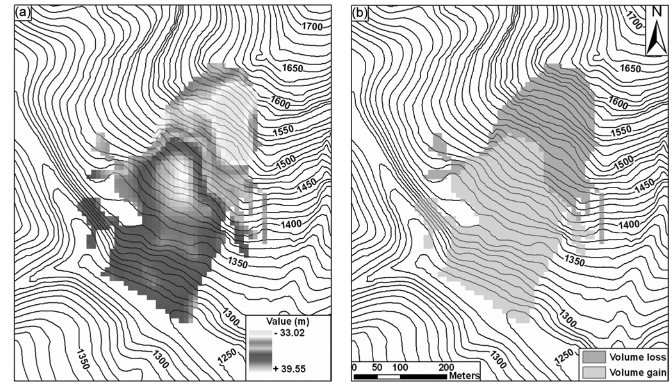

Fig. 4. Volumetric analysis of the Salna landslide. (a) Elevation difference due to landslide with negative values showing the lowering of surface and positive values showing the rising of the surface after the event. (b) Extent of the volume loss and volume gain, which corresponds to the zones of depletion and accumulation, respectively.

TABLE I
Quantitative Comparison of Volume

DEM type	Volume loss (10^6 m^3) Before vegetation correction	Volume loss (10^6 m^3) After vegetation correction	Volume gain (10^6 m^3) Before vegetation correction	Volume gain (10^6 m^3) After vegetation correction	Bulking
DEM (with GCP)	0.77	0.55	1.34	1.43	2.60
DEM (without GCP)	0.76	0.54	1.31	1.41	2.61
DTM (spot height)	0.67		1.26		1.88

So far, we have estimated the landslide volume from DEMs derived with the use of additional GCPs. However, the need for field-measured control points, a strict requirement in traditional photogrammetry, severely undermines the utility of satellite data for rapid and independent postlandslide assessment. To assess the dependence of accurate volume estimation on additional field-mapped GCPs, we also created DEMs only with the RPCs provided with Cartosat-1 data. Such a step is reasonable, as additional GCPs primarily affect the absolute accuracy of the DEM and lessen the relative elevation value distribution. Nevertheless, the effect of integrating two such relative surfaces for accurate change assessment was unknown. Table I shows that the estimated volume values based on RPC-only DEMs fall to within 1%–3% of the GCP-supported DEM values, indicating that the volume figures are less sensitive to GCP support than expected.

The bulking factor (ratio of volume gain to volume loss) of 2.60 (Table I) is comparable with previously reported values for similar events, such as the bulking following the flank collapse of the Casita Volcano, Nicaragua, studied by Scott *et al.* [19]. The bulking of the Salna landslide is due to two factors: 1) incomplete separation of loss area from gain area, due to which the material is still lying at the bottom of the hidden rupture surface [2], which is impossible to be reconstructed from postfailure stereo data (Fig. 3), and 2) poor sorting of large and angular broken quartzite rock fragments [Fig. 1(f)] created by the translational rock slide, leading to a possible overestimation of the gain volume. However, the estimated volume can be considered realistic, since the postlandslide surface was generated shortly (approximately five months) after the occurrence of the landslide, suggesting limited deposition material loss due to surface erosion and further remobilization.

A. *Accuracy Assessment of Volume*

The global accuracy of the DEM has been verified by independent check points, although previous studies have shown that digital photogrammetry with low global errors can still lead to substantial local errors, particularly in areas of low contrast (e.g., uniform vegetation and landslide failure flanks). Volume accuracy assessment in such small local areas is thus a challenge, particularly with only limited reference data, i.e., without a dense network of ground check points for both pre- and postlandslide affected areas. Due to the absence of detailed verification data for the relatively small landslide area (i.e., part of the large DEMs for which accuracy has been checked), we manually extracted spot heights [4], identifying 85 and 129 points from the pre- and postfailure data sets, respectively, using StereoAnalyst in ERDAS Imagine, and compared the volume obtained from spot-height data with the automatic results (Table I). The number of points is sufficient for a reliable comparison since they were collected with particular emphasis on break-in-slope and scarp areas, leading to a surface that models the actual failure area well. Spot heights from the prefailure image were collected by selectively measuring ground elevations in between trees, thus eliminating the need for further vegetation correction, and directly on the failure and deposition surfaces in the postfailure image. These points were interpolated using the TOPOGRID algorithm in ArcGIS to derive reference DTMs [26].

IV. CONCLUSION

Updated elevation data are essential for identifying areas of large-scale topographic changes for disaster management or enforcement of environmental legislation. The purpose of this letter was to assess the potential of a new generation of spaceborne sensors to provide DEMs for the quantification of landscape changes. In this letter, DEMs with 10-m grid size corresponding to two different time periods, generated from Cartosat-1 data using digital photogrammetric methods, were used to quantify large-scale topographic changes resulting from a landslide. Following photogrammetric conventions, we generated DEMs with a grid size equivalent to three to four times of the ground sampling distance. With some data types, such as from SPOT-5, higher resolutions can be achieved, for example, the 2.5-m resolution DEMs produced by Tsutsui *et al.* [9], using superresolution processing [27]. Interestingly, the previously reported requirement for additional GCPs [13] was found to be of lesser importance, allowing us to create surfaces with comparable relative accuracy also without such field-based measurements. This requires the actual coregistration of pre- and postfailure DSMs rather than the use of absolute coordinates. This means that RPCs alone are sufficient for the estimation of volume, thus freeing rapid postfailure volume assessment entirely from field data requirements, although the refinement of the RFM orientation result is required to improve the absolute geolocation accuracy necessary for cartographic applications. Knowledge on prefailure topography is crucial for the accurate estimation of volume [4]. Cartosat-1 was launched in 2005, and its data were systematically acquired, providing substantial archives of images for major parts of the world. The availability of postfailure data sets from Cartosat-1 shortly after the event then enabled us to do rapid volume estimation. The cut-and-fill volumes derived from automatic DEMs showed a reasonably good match with the reference volume derived from DEMs generated using manually extracted spot-height data. This indicates that a 10-m DEM from Cartosat-1 data can be effectively used for large-scale elevation change and volumetric analysis such as that for a deep-seated landslide. The information on landslide volume can effectively be used to establish magnitude–frequency relationship for quantitative estimation of a landslide hazard. However, the volume values calculated based on manually extracted spot heights show deviations of about +18% and −12% for the volume loss and gain areas, respectively, resulting also in a bulking factor that is 27% lower than that based on automatic DEMs with GCPs. These deviations of volume values can be attributed to the steep slope (51°) near the crown of the landslide, where automatically generated DEMs are prone to error [9].

This letter has shown that Cartosat-1 data have the potential to derive volume information critical for disaster assessment, in principle, without any additional GPS field measurement, provided that any present vegetation artifacts are removed from the DEMs used in the change assessment. It must also be noted that, with landslide thickness, i.e., z, typically being the smallest dimension, elevation errors resulting from photogrammetric artifacts or inaccurate DSM-to-DTM correction will have a correspondingly large consequence on volume calculations. The quantitative estimation of similar large-scale changes in the landscape, e.g., due to open-pit mining and urban waste disposal, although not shown in this letter, can, in principle, also be done with Cartosat-1-derived DEMs since they require multitemporal DEMs similar to the ones used in this letter.

REFERENCES

[1] T. R. Martha, A. Guha, K. Vinod Kumar, M. V. V. Kamaraju, and E. V. R. Raju, "Recent coal fire and land use status of Jharia Coalfield, India from satellite data," *Int. J. Remote Sens.*, to be published, to be published. AQ9

[2] C. J. van Westen and F. Lulie Getahun, "Analyzing the evolution of the Tessina landslide using aerial photographs and digital elevation models," *Geomorphology*, vol. 54, no. 1/2, pp. 77–89, Aug. 15, 2003.

[3] A. B. Surazakov and V. B. Aizen, "Estimating volume change of mountain glaciers using SRTM and map-based topographic data," *IEEE Trans. Geosci. Remote Sens.*, vol. 44, no. 10, pp. 2991–2995, Oct. 2006.

[4] N. Kerle, "Volume estimation of the 1998 flank collapse at Casita volcano, Nicaragua: A comparison of photogrammetric and conventional techniques," *Earth Surf. Process. Landforms*, vol. 27, no. 7, pp. 759–772, Jul. 2002.

[5] P. Jaiswal and C. J. van Westen, "Estimating temporal probability for landslide initiation along transportation routes based on rainfall thresholds," *Geomorphology*, vol. 112, no. 1/2, pp. 96–105, Nov. 2009.

[6] P. A. Townsend, D. P. Helmers, C. C. Kingdon, B. E. McNeil, K. M. de Beurs, and K. N. Eshleman, "Changes in the extent of surface mining and reclamation in the Central Appalachians detected using a 1976–2006 Landsat time series," *Remote Sens. Environ.*, vol. 113, no. 1, pp. 62–72, Jan. 2009.

[7] O. Dewitte and A. Demoulin, "Morphometry and kinematics of landslides inferred from precise DTMs in West Belgium," *Natural Hazards Earth Syst. Sci.*, vol. 5, no. 2, pp. 259–265, 2005.

[8] A. Kääb, "Monitoring high-mountain terrain deformation from repeated air- and spaceborne optical data: Examples using digital aerial imagery and ASTER data," *ISPRS J. Photogramm. Remote Sens.*, vol. 57, no. 1/2, pp. 39–52, Nov. 2002.

[9] K. Tsutsui, S. Rokugawa, H. Nakagawa, S. Miyazaki, C. T. Cheng, T. Shiraishi, and S. D. Yang, "Detection and volume estimation of large-scale landslides based on elevation-change analysis using DEMs extracted from high-resolution satellite stereo imagery," *IEEE Trans. Geosci. Remote Sens.*, vol. 45, no. 6, pp. 1681–1696, Jun. 2007.

[10] V. N. Radhika, B. Kartikeyan, B. Gopala Krishna, S. Chowdhury, and P. K. Srivastava, "Robust stereo image matching for spaceborne imagery," *IEEE Trans. Geosci. Remote Sens.*, vol. 45, no. 9, pp. 2993–3000, Sep. 2007.

[11] T. R. Martha, N. Kerle, C. J. van Westen, V. Jetten, and K. Vinod Kumar, "Effect of sun elevation angle on DSMs derived from Cartosat-1 data," AQ10 *Photogramm. Eng. Remote Sens.*, to be published, to be published.

[12] L. Zhang and A. Gruen, "Multi-image matching for DSM generation from IKONOS imagery," *ISPRS J. Photogramm. Remote Sens.*, vol. 60, no. 3, pp. 195–211, May 2006.

[13] E. Baltsavias, S. Kocaman, and K. Wolff, "Analysis of Cartosat-1 images regarding image quality, 3D point measurement and DSM generation," *Photogramm. Rec.*, vol. 23, no. 123, pp. 305–322, Sep. 2008.

[14] *Cartosat-1 Data User's Handbook*, NRSC, Hyderabad, India, [Online]. Available: http://www.nrsa.gov.in/IRS_Documents/Handbook/ AQ11 cartosat1.pdf

[15] R.-F. Chen, Y.-C. Chan, J. Angelier, J.-C. Hu, C. Huang, K.-J. Chang, and T.-Y. Shih, "Large earthquake-triggered landslides and mountain belt erosion: The Tsaoling case, Taiwan," *Comptes Rendus Geosci.*, vol. 337, no. 13, pp. 1164–1172, Sep./Oct. 2005.

[16] D. Loczy, S. Czigany, J. Dezso, P. Gyenizse, J. Kovacs, L. Nagyvaradi, and E. Pirkhoffer, "Geomorphological tasks in planning the rehabilitation of coal mining areas at Pecs, Hungary," *Geografia Fisica E Dinamica Quaternaria*, vol. 30, no. 2, pp. 203–207, 2007.

[17] S. A. Dunning, W. A. Mitchell, N. J. Rosser, and D. N. Petley, "The Hattian Bala rock avalanche and associated landslides triggered by the Kashmir Earthquake of 8 October 2005," *Eng. Geol.*, vol. 93, no. 3/4, pp. 130–144, Aug. 2007.

[18] F. Wang, Q. Cheng, L. Highland, M. Miyajima, H. Wang, and C. Yan, "Preliminary investigation of some large landslides triggered by the 2008 Wenchuan earthquake, Sichuan Province, China," *Landslides*, vol. 6, no. 1, pp. 47–54, Mar. 2009.

[19] K. M. Scott, J. W. Vallance, N. Kerle, J. L. Macías, W. Strauch, and G. Devoli, "Catastrophic precipitation-triggered lahar at Casita volcano, Nicaragua: Occurrence, bulking and transformation," *Earth Surf. Process. Landforms*, vol. 30, no. 1, pp. 59–79, Jan. 2005.

[20] Y. Okura, H. Kitahara, A. Kawanami, and U. Kurokawa, "Topography and volume effects on travel distance of surface failure," *Eng. Geol.*, vol. 67, no. 3/4, pp. 243–254, Jan. 2003.

[21] F. C. Dai and C. F. Lee, "Frequency-volume relation and prediction of rainfall-induced landslides," *Eng. Geol.*, vol. 59, no. 3/4, pp. 253–266, Apr. 2001.

[22] D. Cruden and D. J. Varnes, "Landslide types and processes," in *Landslides Investigation and Mitigation, Special Report 247*, A. K. Turner and R. L. Schuster, Eds. Washington, DC: Transp. Res. Board, Nat. Acad. Sci., 1996, pp. 36–75.

[23] J. Chandler, "Effective application of automated digital photogrammetry for geomorphological research," *Earth Surf. Process. Landforms*, vol. 24, no. 1, pp. 51–63, Jan. 1999.

[24] P. L. Barnard, L. A. Owen, M. C. Sharma, and R. C. Finkel, "Natural and human-induced landsliding in the Garhwal Himalaya of northern India," *Geomorphology*, vol. 40, no. 1/2, pp. 21–35, Sep. 2001.

[25] T. G. Van Niel, T. R. McVicar, L. Li, J. C. Gallant, and Q. Yang, "The impact of misregistration on SRTM and DEM image differences," *Remote Sens. Environ.*, vol. 112, no. 5, pp. 2430–2442, May 2008.

[26] S. M. Wise, "Effect of differing DEM creation methods on the results from a hydrological model," *Comput. Geosci.*, vol. 33, no. 10, pp. 1351–1365, Oct. 2007.

[27] C. Latry and B. Rouge, "Super resolution: Quincunx sampling and fusion processing," in *Proc. Int. Geosci. Remote Sens. Symp.*, 2003, pp. 315–317.

AUTHOR QUERIES

AUTHOR PLEASE ANSWER ALL QUERIES

The paper exceeds the maximum allowable number of pages. Please shorten the paper to fit into five pages.

AQ1 = “DEM” was changed to “DSMs.” Please check if appropriate.
AQ2 = “SAT-PP” was defined as “Satellite Image Precision Processing.” Please check.
AQ3 = This sentence was reworded for clarity purposes. Please check if the original meaning was retained.
AQ4 = Kindly check if the intended meaning of this sentence was achieved.
AQ5 = Please check if the original meaning of this sentence was retained.
AQ6 = Please provide the definition of “GSI.”
AQ7 = Please provide the expanded form of “RS&GIS-AA,” if applicable.
AQ8 = “ETH” was defined as “Eidgenössische Technische Hochschule.” Please check.
AQ9 = Please provide publication update for Ref. [1].
AQ10 = Please provide publication update for Ref. [11].
AQ11 = Please provide year of publication in Ref. [14].
NOTE: Please check the URL provided in Ref. [14]. The page could not be found.

END OF ALL QUERIES